Catalysis Today 441 (2024) 114855

Contents lists available at ScienceDirect

Catalysis Today

journal homepage: www.elsevier.com/locate/cattod

Photoelectrocatalytic application of vanadylporphyrin complexes directly extracted from oil

B.M. Moreno-Torralbo [a], Zh.K. Myltykbayeva [a,b], G. Sánchez-García [c], A. Seysembekova [b], R.M. Fernández-Domene [c], A. Vidal-Moya [a], R. Sánchez-Tovar [c], B. Solsona [c,*], J.M. López Nieto [a,*]

[a] Instituto de Tecnología Química, Universitat Politècnica de València-Consejo Superior de Investigaciones Científicas, Avenida de los Naranjos s/n, Valencia 46022, Spain
[b] Al-farabi Kazakh National University, 71 al-Farabi Ave, Almaty 050040, Kazakhstan
[c] Departament d'Enginyeria Química, Universitat de València, c/ Dr. Moliner 50, Burjassot, Valencia 46100, Spain

ARTICLE INFO

Keywords:
Vanadyl petroporphyrins
Photoelectrocatalysis
Methyl red degradation

ABSTRACT

Non-pure primary Vanadyl petroporphyrins extracted from oil, i.e., PVP(Oil), have been impregnated on SBA-15 or on SiO_2. For comparison, synthetic vanadyl octaethylporphine, VP(S), was also impregnated on the same siliceous materials. The characterization result of unsupported porphyrins and the catalysts, by FTIR and DR-UV–vis, confirm the successful incorporation of the corresponding vanadyl porphyrins. Electrochemical and photoelectrochemical properties of these catalysts have been evaluated through Electrochemical Impedance Spectroscopy (EIS), Mott-Schottky (MS) and voltammetry tests. According to the results, primary vanadyl porphyrin extracted from oil, PVP(Oil), show better photoelectrochemical response, regardless of the support used (either SiO_2 or SBA15), than synthetic ones, VP(S). Additionally, this study reveals that PVP(Oil) can be used as photoelectrocatalysts for methyl red (MR) degradation (a common organic dye), showing almost a complete degradation of (MR) using PVP(Oil)-SBA15 catalyst after 3 h. Interestingly, an increase of more than 25% in the kinetic constant for the photoelectrochemical degradation of MR is shown for the PVP(Oil) in comparison to the VP(S).

1. Introduction

Metalloporphyrins, in which the porphyrins act as multifaceted ligands coordinating metals (providing rigid and stable coordination environments of metals), show particular physicochemical characteristics and their application is due, in part, to the tunable activity, chemical inertness, and structural stability [1–4]. This is the case of their use in biomedical applications, solar cells, nanowires/nanomotors or energy storage [1–4], but also as catalysts and photocatalysts [1,5–13], some of them supported/encapsulated [13–17], or incorporated into MOFs [18–22].

V-porphyrins based catalysts have been also proposed as effective catalysts in oxidation, epoxidation, deoxygenation or hydrogenation reactions [23–27], some of them with electrocatalytic performance [28]. However, so far, such studies have been carried out with materials with synthetic porphyrins [29].

Vanadium is usually the most abundant trace metal in crude oils. According to the U.S. Geological Survey, bitumens, heavy oils, and medium and light crude oils contain averages of 340, 180, 33 and 8 ppm of vanadium [30]. In these cases, it is commonly present in porphyrin structures as the vanadyl ion (VO^{2+}) forming coordination complexes (i.e., vanadyl porphyrins) [31]. These trace metals in crude oils have a negative effect on the refining process and reduce the value due to processing needed. Accordingly, there is a need of removing the metals from the porphyrins and/or performing an extraction to eliminate the V-containing porphyrins. Thus, in the latter case, it is of paramount importance to look for new applications for the Vanadyl petroporphyrins, especially taking into account the possibility of obtaining these compounds by extraction [29–39]. Typically, vanadyl porphyrins compounds usually found in crude oil include etioporphyrin (ETIO) and

* Corresponding authors.
E-mail addresses: benjamin.solsona@uv.es (B. Solsona), jmlopez@itq.upv.es (J.M. López Nieto).

https://doi.org/10.1016/j.cattod.2024.114855
Received 12 February 2024; Received in revised form 17 May 2024; Accepted 28 May 2024
Available online 29 May 2024

deoxophyllerithro-etioporphyrins (DPED), although other, such as protoporphyrins (RHODO) or benzoetioporphyrins (Benzo), can be also observed [32].

Vanadyl porphyrins present interesting electrical properties [28, 40–44], so vanadium-containing petroporphyrins could be of interest for use as catalysts in electrochemical and/or photoelectrochemical reactions.

Herein, we report a new approach on the use of vanadyl-containing petroporphyrins. In this way, different catalysts have been prepared based on V-containing petroporphyrins, extracted from oils of the North Buzachi region, which were deposited on SiO_2 or encapsulated into mesoporous SBA-15. For comparative purposes, catalysts based on synthetic octaethylporphyrin vanadium (IV) oxide, VP(S), deposited in silica or encapsulated in the mesoporous silica material, have been also prepared. The catalysts were characterized by several physico-chemical techniques, including electrochemical techniques, and tested in photoelectrochemical applications.

2. Experimental

2.1. Materials

Vanadyl octaethylporphine (2,3,7,8,12,13,17,18-Octaethyl-21*H*,23*H*-porphine vanadium(IV) oxide, named as **VP(S)**), $C_{36}H_{44}N_4OV$, was purchased from Aldrich. Pluronic (P123, Sigma Aldrich), hydrochloric acid (HCl, 37%; Fisher Chemical), butanol (Sigma Aldrich) and tetraethyl orthosilicate (TEOS, Sigma Aldrich) were used in the synthesis of mesoporous materials. SiO_2 nanopowder (surface area of 225 $m^2\ g^{-1}$, from (Aldrich).

Primary vanadylporphyrin concentrate from oils of the North Buzachi region were extracted at 20°C using N,N-dimethylformamide (DMF) [37], see also supporting information. This will be named as **PVP(Oil)**. As a reference, **R(oil)** sample corresponds to a fraction obtained during the extraction of vanadyl complexes in which no vanadyl compound was observed.

Mesoporous materials, SBA-15 structure, were synthesized according to a procedure previously reported [45]. The solid formed was filtered and washed with 2 L of deionized water, drying it at 60 ºC for 12 hours and finally calcined (at 550 ºC for 4 hours, 1.5 ºC min^{-1} ramp) in order to eliminate the remaining organic template.

2.2. Preparation of porphyrins-containing siliceous materials

V-porphyrins (either VP(S) or PVP(Oil)) have been deposited on two different siliceous materials (silica or SBA-15) through an impregnation method. **PVP(Oil)** or **VP(S)** were stirred for 6 h at 65 °C in a methanolic media (Methanol/**PVP(Oil)** or methanol/**VP(S)** mass. ratio of 100) in the presence of the support (silica or SBA-15) and then rotaevaporated in vacuum at 65 ºC until a slightly humid solid was obtained. These mixtures were dried overnight in an oven at 60ºC. The samples supported on SBA-15 will be named as PVP(Oil)-SBA15 or VP(S)-SBA15, respectively, with a porphyrin or primary porphyrin content of ca. 10 wt%. The samples supported on amorphous silica will be named as PVP(Oil)-SiO_2 or VP(S)-SiO_2, respectively, also with a porphyrin or primary porphyrin content of ca. 10 wt%. The characteristics of porphyrin-containing siliceous materials are shown in Table 1.

2.3. Characterization of catalysts and supports

The specific surface area of catalysts and supports have been determined by BET method from N_2 adsorption isotherms at -196 ºC measured in a Micromeritics TriStar 3000 instrument.

IR spectra were measured with a Nicolet 205xB spectrophotometer (at a spectral resolution of 1 cm^{-1} and 128 accumulations per scan) in the 450–4000 cm^{-1} region. Dried catalysts (ca. 20 mg) were mixed with 100 mg of dry KBr and pressed into a disk (600 kg cm^{-2}). In the case of unsupported vanadyl porphyrins, they were analyzed using samples diluted in CH_2Cl_2.

Diffuse Reflectance UV–vis (DR-UV–vis) spectra were recorded within the 200–800 nm range using a *Varian* spectrometer model Cary 5000. In the case of unsupported vanadyl porphyrins, they were analyzed using samples diluted in CH_2Cl_2.

EPR spectra were obtained at -170ºC using an EMX-12 Bruker spectrometer and working at the X band, with a frequency modulation of 100 kHz and 1 G amplitude.

2.4. Electrochemical measurements

Electrochemical and photoelectrochemical properties of porphyrin samples have been extensively studied through different techniques: electrochemical impedance spectroscopy (EIS) measurements, Mott-Schottky (MS) analysis and cyclic voltammetries and linear voltammetry applying dark-light pulses. The experiments were carried out in a three-electrode configuration cell using a 0.1 M Na_2SO_4 aqueous solution as electrolyte, except for the cyclic voltammetries, where the electrolyte was 10 mM $Fe(CN)_6K_4$ + 0.1 M Na_2SO_4. The working electrode consisted of the VP catalyst deposited on a conductive FTO (fluorine-doped tin oxide) with an exposed surface area to the electrolyte of 0.5 cm^2. An Ag/AgCl (3 M KCl) electrode was used as reference and a platinum wire as counter electrode. A potentiostat (Palmsens 4) was used to conduct the tests. For the photoelectrochemical tests, a laser with a wavelength of 365 nm and a power of 100 mW·cm^{-2} was used.

EIS experiments were carried out at 0.3 V (vs. Ag/AgCl) over a frequency range from 100 kHz to 10 mHz with a signal amplitude of 0.01 V. Mott-Schottky analyses were carried out at a frequency value of 5 kHz by sweeping the potential from 0.5 to −0.5 V, with an amplitude signal of 0.01 V. Cyclic voltammetries were performed from -0.1 V to 0.6 V at 10 mV s^{-1}.

Photocurrent density as a function of the applied potential was registered by chopped light radiation (60 s dark/20 s light) with a potential scan from 0.24 V to 1.02 V.

Vanadyl porphyrins were used as catalysts in the photoelectrochemical degradation of methyl red (MR) dye using sulfuric acid 0.1 M as supporting electrolyte. A glass cell with a quartz window and three electrodes immersed in the dye solution was used to perform the photoelectrodegradation. The VPs were used as working electrode (with an exposed area of 2.85 cm^2), a platinum tip as counter electrode and an Ag/AgCl electrode as reference. Experiments were carried out applying

Table 1
Characteristics of catalysts.

Catalyst	Origin of Porphyrin	S_{BET} ($m^2\ g^{-1}$)[a]	Amount of V^{4+} by EPR	R_1 (kΩ·cm^2)[b]	i_A (μA cm^{-2})[c]
PVP(Oil)-SiO_2	Extracted from Oil	234	0.16	0.57	582.5
PVP(Oil)-SBA15	Extracted from Oil	700	0.15	22.05	534.9
VP(S)-SiO_2	Synthetic	337	1.15	17.29	537.9
VP(S)-SBA15	Synthetic	710	1.21	0.94	657.6

[a] Surface area determined from N_2 adsorption isotherms;
[b] Values of the interfacial charge-transfer resistance (R1) for the different porphyrin catalysts;
[c] Anodic current density values for the different porphyrin catalysts obtained from voltametric curves.

1 $V_{Ag/AgCl}$ with a potentiostat (Palmsens 4) illuminating the sample with an UV lamp (wavelength of 365 nm).

Dye degradation was monitored at 30 min at first and then, every hour for 3 h using a quartz cell in a spectrophotometer (Cecil CE 1011) at a wavelength of 517 nm.

3. Results and discussion

3.1. Characterization of the catalysts

The catalysts supported on SiO_2 or SBA-15 have been characterized by several techniques and the results are summarized in Table 1. We must indicate that the vanadyl porphyrins deposited over mesoporous materials show XRD patterns at low angles similar to that observed in the porphyrin-free material (Fig. S1, supporting information). On the other hand, the XRD patterns of materials deposited on SiO_2 do not present representative lines of the corresponding porphyrins indicating that they are highly dispersed. This is in agreement with previous results in which samples with porphyrins content lower than 10 wt% cannot be studied by this technique [28].

Fig. 1 shows the IR spectra of primary vanadyl porphyrin concentrate directly extracted from oil with N,N-dimethylformamide (DMA), i.e., **PVP(Oil)** sample (Fig. 1, spectrum a). For comparison, it has been also included the IR spectra of synthetic porphyrin, i.e., **VP(S)** sample (Fig. 1, spectrum b), whereas the IR spectra of the reference **R(Oil)** sample is presented in Fig. S2A.

In the case of unsupported **PVP(Oil)** sample, it can be seen the presence of characteristics C–H groups, with bands at ca. 2956, 2927, and 2856 cm^{-1} (with a shoulder at 2868 cm^{-1}), in addition to those at 1443, 1372, and 705 cm^{-1} [29,35,46], which are related to asymmetrical CH_2, symmetrical CH_2 and CH_3 asymmetric stretching, respectively. Furthermore, other IR bands at 1724, 1602 1450, 1372, 1281, 1263, 1120, 1071, 1025, 1017 and 854 cm^{-1} are also observed in the vanadyl porphyrin complexes extracted from oil. Small differences have been

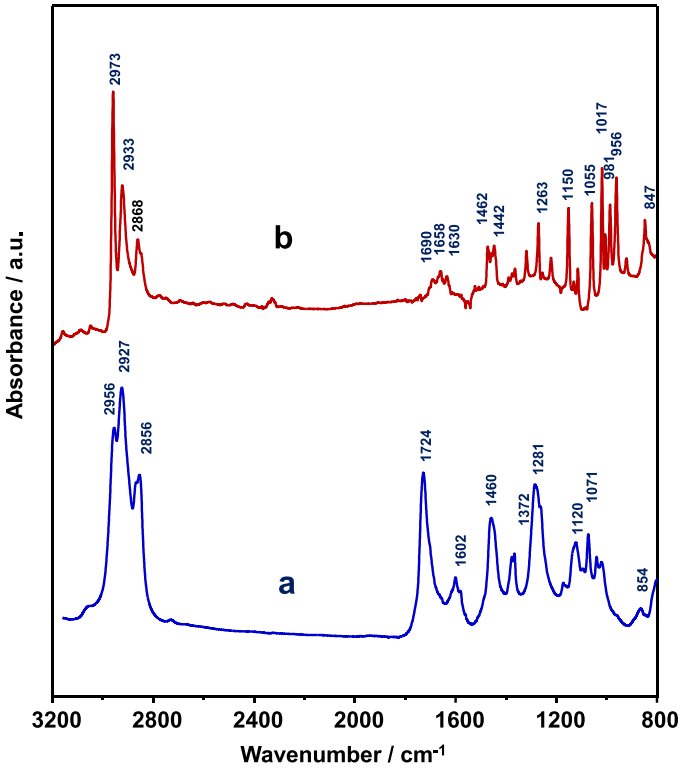

Fig. 1. IR spectra of vanadyl porphyrin complexes directly extracted from oil, **PVP(Oil)** (a); and the synthetic porphyrin, **VP(S)** (b).

observed for the unsupported **R(Oil)** sample (Fig. S2A), especially the absence of band at 1724, 1281, 1263, 1120, 1071, 1025, 1017 and a different intensity of bands at 2865 and 2856.

On the other hand, the IR spectrum of the synthetic V-porphyrin, **VP(S)** sample, presents bands at ca. 2967, 2930 and 2868 cm^{-1} (with a shoulder at 2856 cm^{-1}), in addition to those at 1690, 1658, 1630, 1462, 1442, 1623, 1150, 1055, 1017, 981, 956 and 847 (Fig. 1, spectrum b). The intensity of the bands in the 3000–2800 interval is similar to those reported previously for octaethylporphyrins-containing materials [43,47].

We must indicate that the intensities of the three bands and the shoulder in the 2800–3000 cm^{-1} region change from **PVP(Oil)** sample (with the following trend: $I_{2927} > I_{2956} > I_{2856} > I_{2868}$), as reported previously [29,35], or **R(Oil)** (with the following trend: $I_{2927} > I_{2956} > I_{2868} > I_{2856}$) to **VP(S)** sample (with the following trend: $I_{2973} > I_{2933} > I_{2868} > I_{2856}$) [43,47]. Accordingly, the presence of these porphyrins in supported materials cannot be easily observed by comparing only the intensity of bands in the 3000–2850 cm^{-1} range.

In the case of supported V-free material (Fig. 2, and Fig. S2B), it can be also observed the same trend in the intensity of the four bands in the 3000–2850 cm^{-1} range that those observed for the corresponding unsupported materials.

Fig. 3 shows the DR-UV–vis spectra of unsupported vanadyl porphyrins, i.e., **PVP(Oil)** sample (Fig. 3, spectrum a) and **VP(S)** sample (Fig. 3, spectrum b). For comparison, it has been also presented DR-UV–vis spectrum of the reference V-free material, i.e., **R(Oil)** (Fig. S3A, in supporting information). The samples were diluted in CH_2Cl_2, as suggested by other authors [32,38,39,46,48–51].

The presence of the Soret band at ca. 408 nm indicates that both **PVP(Oil)** and **VP(S)** samples contain Vanadyl porphyrin complexes [38,39,46,51], whereas no vanadyl porphyrin is present in the **R(Oil)** sample (Fig. S3A). In addition, the important absorption in the short-wave part of the spectrum for the **PVP(Oil)** and **R(Oil)** samples corresponds to non-porphyrin impurities [38,39,46,51], given that vanadyl porphyrins have a very low absorption in the UV region. Accordingly, **PVP(Oil)** sample present vanadyl porphyrin complexes in addition to impurities, whereas **R(Oil)** samples represent a V-free material with similar impurities than that in **PVP(Oil)** sample (as observed also by IR).

In the case of V-containing materials, it can be elucidated the presence of three bands at 407, 535, and 570 nm (Fig. 3, spectrum a) and at 408, 532, 571 nm (Fig. 3, spectrum b), which are also observed in other V-porphyrins when diluted in dichloromethane or in tetrahydrofuran [32,46–50].

In fact, the band at ca. 407 nm correspond to the Soret band, while the bands at ca 530 and 570 nm can be assigned to β- and α-bands, respectively [38,39,46,47–53]. In this way, it has been proposed that the Soret band varies from 406, 407, 410 and 414 when comparing vanadyl derivates of etioporphyrin, octaethylporphyrin, deoxophylloerythroetioporphyrin or benzoetioporphyrin, respectively; whereas the β- and α-bands vary from 532 to 544 and 570–578, respectively [32,34–39,46,47–53]. However, changes in Soret and Q bands can be induced by perturbation of the electronic structures, such as protonation, metal chelation, and substituents [34,36]. We must indicate that the intensity of bands related to the α- (I_{570}) and β-bands (I_{530}) change depending on the nature of porphyrin. Thus, the I_{570}/I_{530} ratio in **VP(S)** sample is higher than that observed in **PVP(Oil)** sample.

Fig. 4 and Fig. S3 (in supporting information) shows the DR-UV–vis spectra of catalysts. In all cases, it can be observed the presence of bands at 400, 530 and 570 nm, suggesting no changes when the vanadyl porphyrins were deposited on siliceous materials. In addition, and as observed for unsupported porphyrins, the intensity of the bands related to the α- (I_{570}) and β-bands (I_{530}) changes, being the I_{570}/I_{530} ratio on **VP(S)**-containing catalysts (Fig. 4, spectra c and d) higher than those observed in **PVP(Oil)**-containing catalysts (Fig. 4, spectra a and b).

We must indicate that, in the case of the sample **R(Oil)** supported on SBA-15, (i.e., R(Oil)/SBA15) no bands in the 400–600 range have been observed (Fig. S4). Accordingly, no vanadium is present in this material,

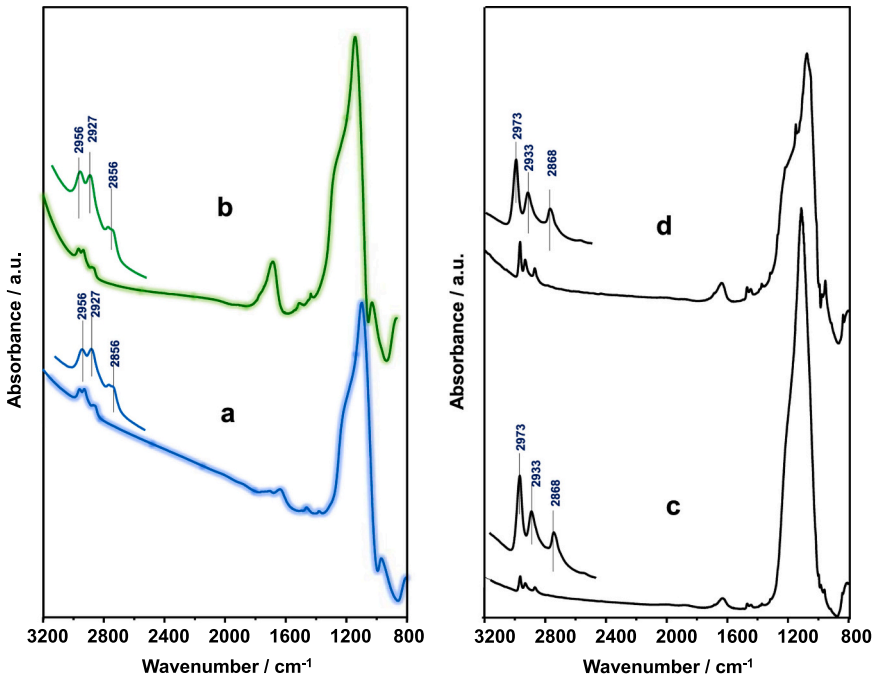

Fig. 2. IR spectra of vanadylporphyrin complexes deposited on siliceous materials: a) PVP(Oil)-SiO_2; b) PVP(Oil)-SBA15; c) VP(S)-SiO_2; d) VP(S)-SBA15.

X-band spectra of supported V-porphyrin catalyst are comparatively shown in Fig. 5, whereas the quantification of V(IV) by EPR is also presented in Table 1. For comparison, the EPR spectrum of V-free extract from oil has been also included (Fig. 5, spectrum e).

As one can see in Fig. 5, the hyperfine patterns corresponding to parallel and perpendicular orientations of the complex relative to the magnetic field largely overlap at X-band EPR. All of them present typical EPR spectra with neatly resolved ^{51}V hyperfine lines at 120 K, consisting of eight broad lines separated by about (175 gauss) that can be ascribed to the 8-line hyperfine structure from the 51 V (I = 7/2) nucleus [54–56]. However, significant differences are observed between VP (S)-containing samples (Fig. 5, spectra a and b) and PVP (Oil)-containing samples (Fig. 5, spectra c and d). In this way, the EPR spectra of VP(S)-containing samples present spectra with a higher bandwidth than those observed for PVP(Oil)-containing samples. Similar results have been previously observed [54], in which in solid with low dispersion, as occurs in VP(S)-containing samples, the spin concentration is high and hence the lines are broadened by the exchange interaction between the spins. In addition, VP(S)-containing samples present $g_{\|}$ and $g_{\perp}$ value of 1.962 and 1.977, respectively, with $A_{\|}$ and $A_{\perp}$ values of 173.2 gauss and 57.3 gauss, respectively. However, PVP (Oil)-containing samples present). Fig. 4b shows a detailed spectrum of sample 20VP@SBA, with $g_{\|}$ and $g_{\perp}$ value of 1.960 and 1.970, respectively, with $A_{\|}$ and $A_{\perp}$ values of 166.0 gauss and 56.0 gauss, respectively.

In this way, the EPR results of a VP(S)-SBA15 sample, with a VP content of ca. 1.5 wt% (and a VO^{2+} content of ca. 0.35) (Figure S5), present a hyperfine signal similar to that observed for PVP(Oil)-containing samples. However, two type of signal can be deduced, which correspond with those observed in both VP(S) and PVP(Oil)-containing samples.

On the other hand, V-free extract from oil (Fig. 5, spectrum e), does not indicate the presence of vanadyl species. However, the presence of organic free radical as minority cannot be ruled out [54].

3.2. Electrochemical and photoelectrochemical properties

Electrochemical and photoelectrochemical properties of porphyrin samples have been extensively studied through different techniques: EIS, MS analysis, cyclic voltammetry and linear voltammetry applying dark-light pulses.

Fig. 6 shows the EIS results in the form of Nyquist (Fig. 6A) and Bode-module (Fig. 6B) plots, while the corresponding Bode-phase plots are presented in Fig. S6A. For comparison, the electrochemical characteristics of V-free extract from oil supported on SBA-15 (R(Oil)-SBA) have been also presented in Fig. S7.

In Nyquist plots (Fig. 6A), two incomplete semicircles can be observed for all the samples, the amplitude of the first one (at intermediate frequencies) being lower than that of the second one (at low frequencies). Comparing the response of the different catalysts, it can be seen that the synthetic VP(S)-SiO_2 sample presented the lowest impedance values, followed by the samples supported in SBA15 (i.e., VP(S)-SBA15 and PVP(Oil)-SBA15) and, finally, the sample PVP(Oil)-SiO_2, whose last semicircle was the largest. We must inform that observing Bode-phase plots (Fig. S2), two phase angle peaks are discerned for all the catalysts, which is consistent with the two semicircles observed in Nyquist plots at intermediate and low frequencies.

On the other hand, from Bode-module plots (Fig. 6B), the total resistance of the system (R_T) can be estimated at the lowest frequency value. In this case, the trend of the total resistance of the system increases as follow: VP(S)-SiO_2 < PVP(Oil)-SBA15 < VP(S)-SBA15 < PVP (Oil)-SiO_2). A similar trend has been also observed when comparing the Nyquist plots.

To obtain the resistance of the different elements of the electrochemical system formed at the interface between supported porphyrins and the electrolyte, EIS results have been fitted to an electric equivalent circuit (Fig. S6-B; supporting information), formed by two R-CPE elements associated in series, together with a previous resistance (R_S), related to the electrolyte. In this circuit, subscript "1" refers to the electrical behavior of porphyrins while subscript "2" indicates the properties of the underneath support (SiO_2 or SBA). For the purposes of this study, the most interesting resistance is that related to the charge-transfer processes taking place at the porphyrin/electrolyte interface (R_1), since porphyrins are the active materials. Values of these resistances are shown in Table 1. In this case, catalysts with the lowest R_1 value are the PVP(Oil)-SiO_2 and the VP(S)-SBA15, with similar values. The other two catalysts (i.e., VP(S)-SiO_2 and PVP(Oil)-SBA15) presented much higher R_1 values. We want to indicate that the V-free extract from

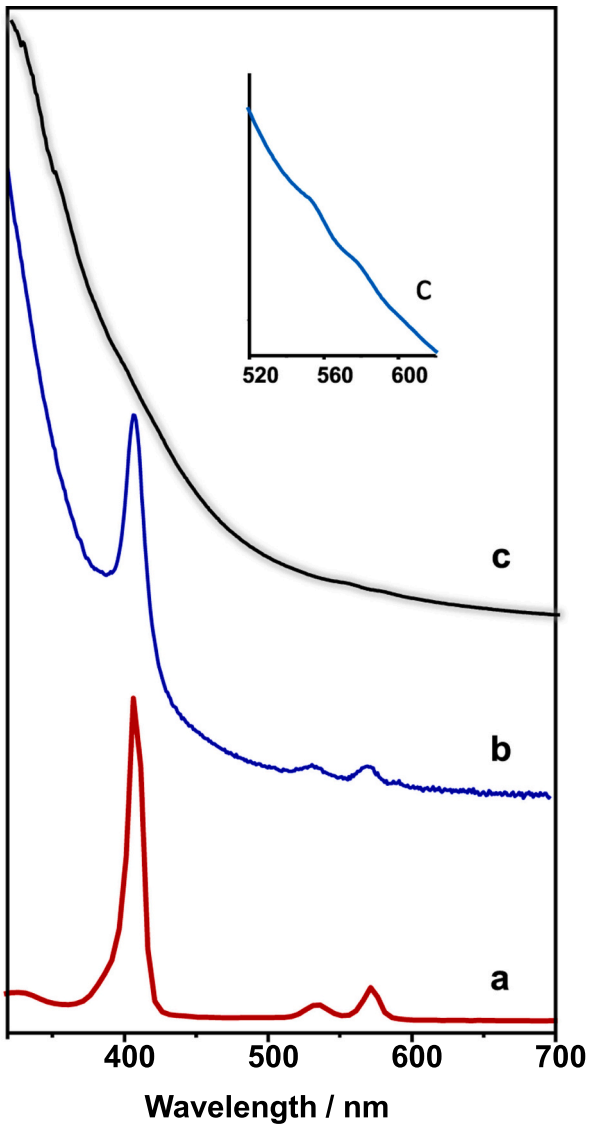

Fig. 3. DR-UV–vis spectra of unsupported porphyrins: a) **VP(S)** sample; b) **PVP (Oil)** sample; c) **R(Oil)** sample. The samples were diluted in CH_2Cl_2 (ca. 2 mg of porphyrinic precursor in 20 mL of CH_2Cl_2).

oil supported on SBA-15 (R(Oil)-SBA) presents the highest charge transfer resistance (Fig. S7).

To investigate the semiconducting properties of the porphyrin-based catalysts, Mott-Schottky plots have been plotted and presented in Fig. 7A. For comparison the electrochemical results of V-free extract from oil (R(Oil)-SBA) has been also presented in Fig. S7-C.

All the samples exhibit n-type semiconducting behavior, since linear regions with positives slopes are obtained in all cases. It can be seen that higher slopes were obtained for real petroleum-extracted porphyrins, indicating lower density of defects (donor species), according to Mott-Schottky equation:

$$\frac{1}{C^2} = \frac{1}{C_H^2} + \frac{2}{\varepsilon_r \varepsilon_0 e N_D}\left(E - E_{FB} - \frac{kT}{e}\right)$$

being C is the capacitance at the interface, C_H is the capacitance of the Helmholtz layer, ε_r is the dielectric constant of the sample, ε_0 is the vacuum permittivity ($8.85 \cdot 10^{-14}$ F/cm), e is the elementary (electron) charge ($1.60 \cdot 10^{-19}$ C), N_D is the density of defects (donor species for n-type semiconductors), E is the applied potential, E_{FB} is the flat-band potential, k is the Boltzmann constant ($1.38 \cdot 10^{-23}$ J/K) and T is absolute temperature. Therefore, the higher slopes for the real porphyrins indicate lower N_D values and, hence, a lower degree of defectiveness within their structures. The presence of defects, which are located between the valence and the conduction band, might act as carrier traps (trapping electrons or holes) and then, the efficiency of the catalyst in the photoelectrochemical application is reduced.

Cyclic voltammetries of the samples were performed in order to investigate electrochemical behavior of porphyrin-based catalysts in terms of kinetics, since anodic and cathodic current densities are directly associated with the rate of charge-transfer processes. The results are presented in Fig. 7B. In general, it can be seen two clear peaks; one anodic (oxidation) centered at approximately 0.3–0.35 V, and another cathodic (reduction) centered at c.a. 0.15 V. In order to use these catalysts as (photo)anodes, anodic current densities (i_A) are the important ones. Therefore, these values are presented in Table 1. According to these data, samples with the highest i_A values (VP(S)-SBA15 and VP (Oil)-SiO_2) are the samples whose interfacial charge-transfer resistance R_1 was the lowest (see Table 1), which is consistent, since lower charge-transfer resistances result in higher current densities.

Photoelectrochemical characterization was also carried out. In this case, linear voltammetries were recorded applying at the same time dark-light pulses, to obtain dark current density values and photocurrent density values. Fig. 8 shows the corresponding curves, whereas the results for R(Oil)-SBA sample are presented in Fig. S7-E.

First, catalysts based on synthetic porphyrins (i.e., VP(S)-based materials) provided significantly lower photocurrent densities (smaller pulses), while petroleum-extracted porphyrins gave significantly higher photocurrent density values. In Table 2, values of dark current densities (i_{dark}), photocurrent densities (i_{light}) and net current densities obtained as $\Delta i = i_{light} - i_{dark}$ are presented. Again, petroleum extracted catalysts, unsupported **PVP(Oil)** presented the highest net current density values (especially the one supported in SBA15), much higher than those for the synthetic porphyrins, i.e., unsupported **VP(S)**. This behavior may be related to the lower defectiveness (low density of defects located between the valence and the conduction band) of natural (petroleum-extracted) samples, as explained above when describing Mott-Schottky analysis results. Therefore, in this case, a lower density of defects led to a better photoelectrocatalytic performance, since these defects could act as recombination centers of photogenerated electrons and holes, therefore decreasing the catalysts efficiency [57,58].

3.3. Photoelectrocatalytic degradation of methyl red

It has been also studied the photoelectrocatalytic degradation of methyl red over porphyrin-based catalysts, by considering the three different catalytic approaches: photoelectro-, photo- and electro-catalytic degradation. In this way, the absorbance intensity of methyl red in 0.1 M H_2SO_4, which was used as supporting electrolyte, has been presented in Fig. S8 (supporting information). There, the typical absorbance peak of methyl red centred at ~517 nm (reference band of methyl red in acid media) can be clearly observed, which is the responsible for the red colour of the azo dye [59,60]. Therefore, the evolution of this absorbance peak was followed with time using the vanadyl porphyrins as catalysts.

Fig. 9A presents, comparatively, the time evolution of the ratio between the methyl red absorbance peak (or concentration) at ~517 nm at a given time (during 3 h) and the initial methyl red absorbance (or concentration equal to 40 ppm), C/C_0, for the three different catalytic approaches (photoelectro-, photo- and electrocatalytic) using the petroleum extracted vanadyl porphyrins supported in SBA15 (**VP(Oil)-SBA15**), since this sample offered the best photoelectrochemical response (see Fig. 8).

The decolouration efficiency under those experimental conditions is shown in Fig. 9B. It can be observed that low values of C/C_0 and high values of decolouration efficiency were achieved with the

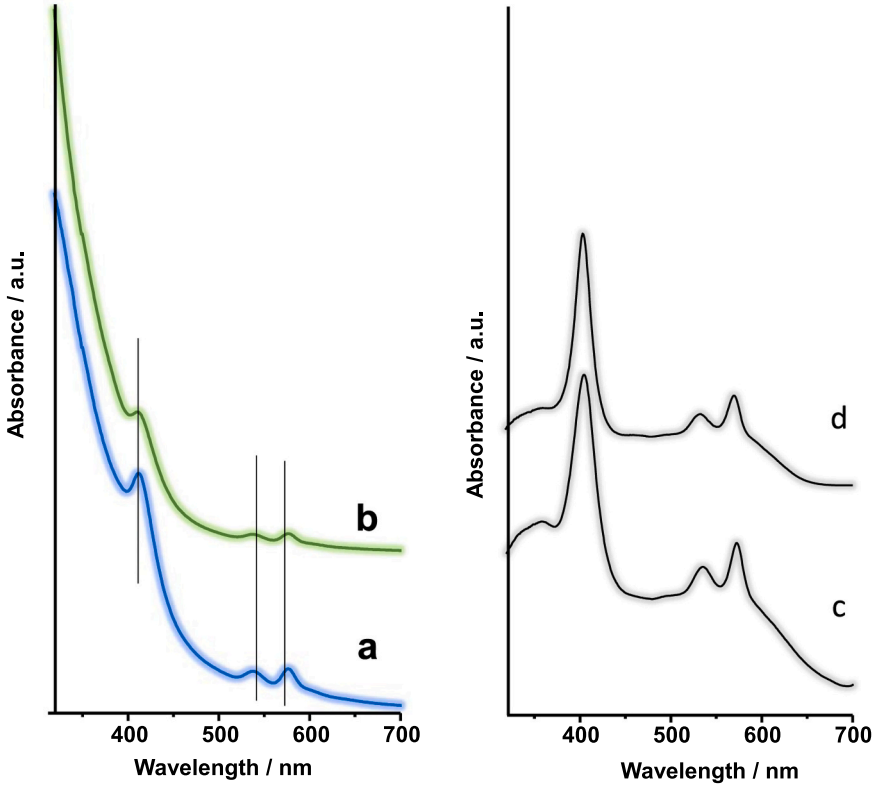

Fig. 4. DR-UV–vis spectra of vanadyl porphyrin complexes deposited on siliceous materials: a) PVP(Oil)-SiO_2; b) PVP(Oil)-SBA15; c) VP(S)-SiO_2; d) VP(S)-SBA15.

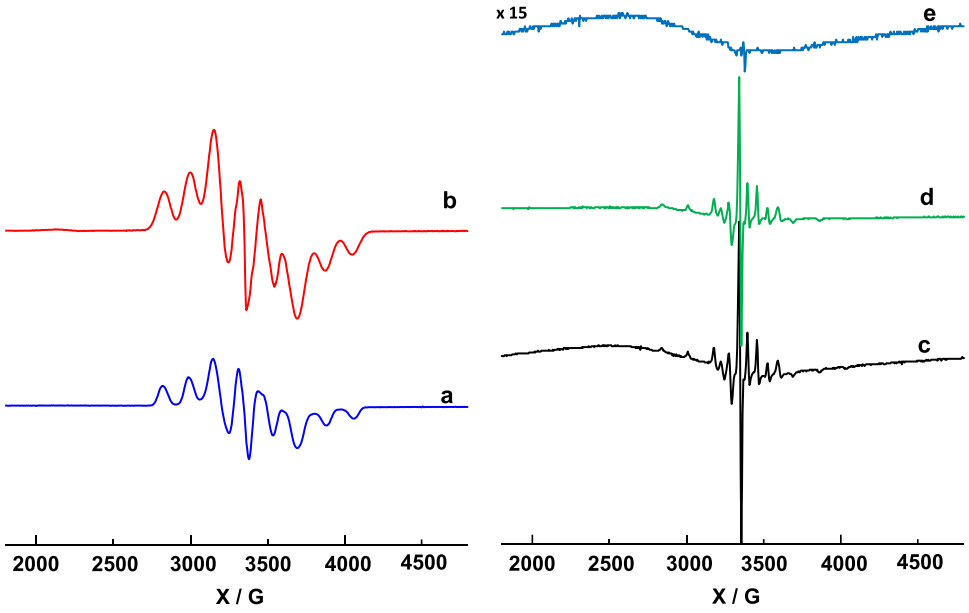

Fig. 5. EPR spectra of catalysts: a) VP(S)-SiO_2; b) VP(S)-SBA15; c) PVP(Oil)-SiO_2; d) PVP(Oil)-SBA15. For comparison, the EPR spectra of V-fee material extract from oil, R(Oil)-SBA (e), is also included.

photoelectrocatalytic approach after 3 hours, showing degradation efficiencies higher than 98% in comparison to the photo or the electro reactions, with decolouration values of 75 or 47%, respectively. Therefore, the use of the combined photoelectrocatalytic approach with a petroleum-extracted VP makes possible to perform a rapid discoloration of the solution. This is a very interesting result, since a petroleum-waste could be reused for an easy and fast removal of a recalcitrant organic dye, contributing to sustainability and circular economy.

Additional tests were carried with the photoelectrocatalytic system in order to compare the degradation efficiency of the dye using a synthetic vanadyl porphyrin also supported in SBA15, i.e., VP(S)-SBA15.

Fig. 10A shows the comparison between C/C_0 vs. *time* plots for both porphyrins (synthetic and petroleum-extracted), where C_0 is the initial methyl red concentration (40 ppm) and C is the methyl red concentration at time t obtained from absorbance values at 517 nm. It can be observed that the absorbance peak decreased significantly slower for VP

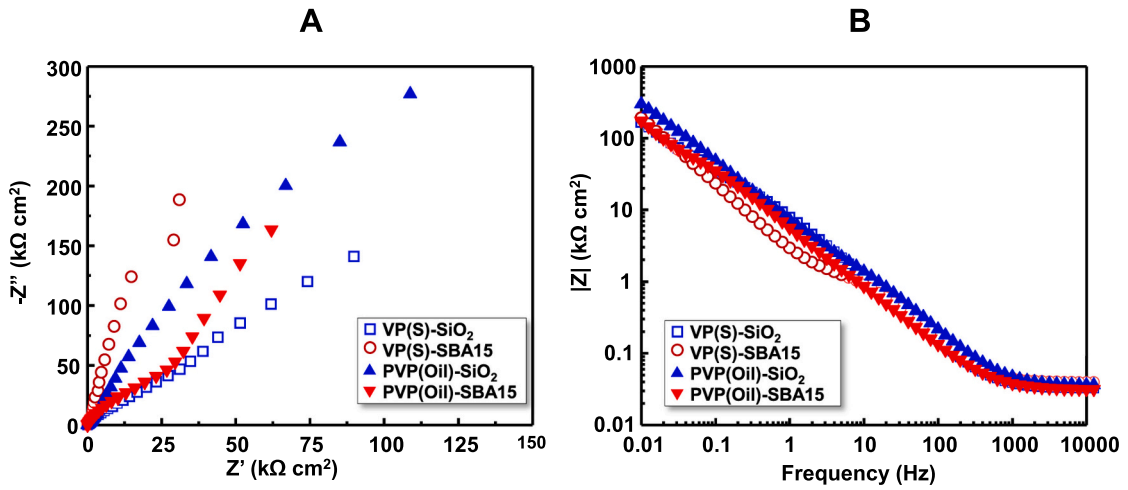

Fig. 6. Nyquist (A) and Bode-module (B) plots for the different porphyrin-based catalysts: PVP(Oil)-SiO_2; PVP(Oil)-SBA15; VP(S)-SiO_2; VP(S)-SBA15.

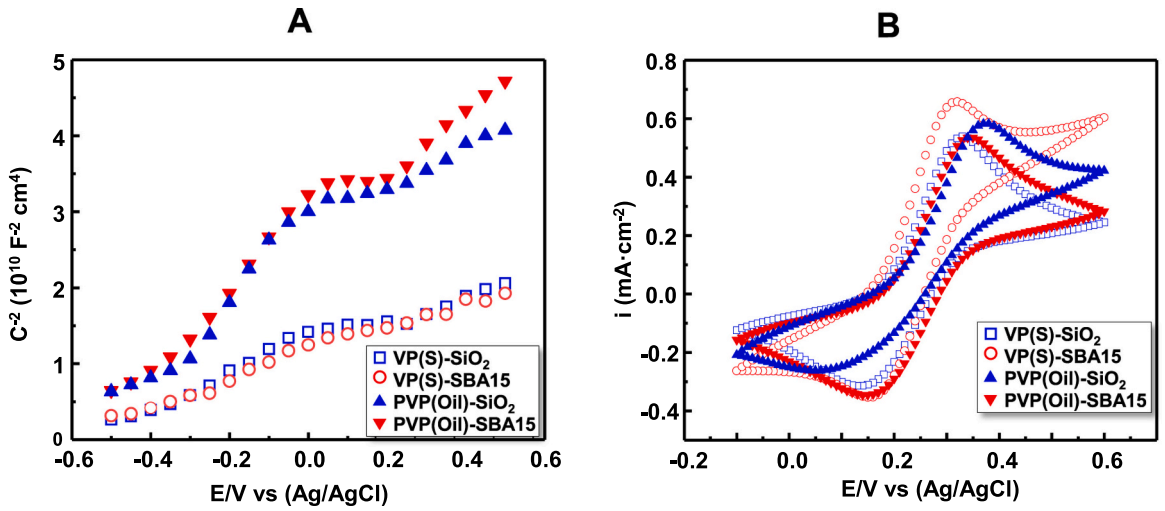

Fig. 7. Mott-Schottky plots (A) and Cyclic voltammetries (B) for the different porphyrin-based catalysts.

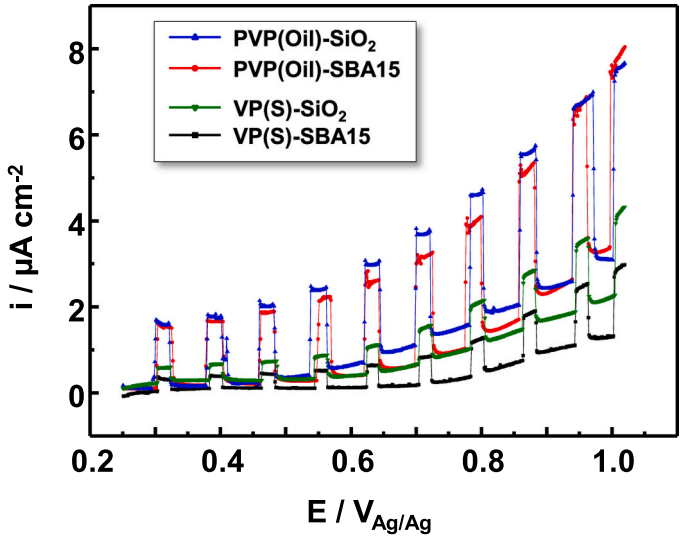

Fig. 8. (Photo)current density vs potential curves for the different porphyrin catalysts, obtained by applying dark-light pulses.

Table 2
Dark current densities, photocurrent densities and net current densities obtained at different potential values for the different porphyrin catalysts.

Catalyst	Potential ($V_{Ag/AgCl}$)	i_{dark} ($\mu A \cdot cm^{-2}$)	i_{light} ($\mu A \cdot cm^{-2}$)	Δi ($\mu A \cdot cm^{-2}$)
PVP(Oil)-SiO2	0.40	0.22	1.74	1.52
	0.55	1.16	2.46	1.30
	0.70	2.76	3.74	1.35
PVP(Oil)-SBA15	0.40	0.24	1.66	1.42
	0.55	0.40	2.22	1.82
	0.70	0.92	3.24	2.32
VP(S)-SiO2	0.40	0.30	0.78	0.48
	0.55	0.54	1.12	0.58
	0.70	1.25	2.15	0.90
VP(S)-SBA15	0.40	0.10	0.39	0.29
	0.55	0.10	0.50	0.40
	0.70	0.25	0.85	0.60

(S)-SBA15 catalysts (the synthetic vanadyl porphyrin) than for PVP(Oil)-SBA15 catalysts (the petroleum-extracted one). According to these results, degradation was more efficient using the VP(Oil)-SBA15 catalyst. Degradation efficiency (Fig. 10B) increased from 0% in the case of the synthetic V-porphyrin-containing material (i.e., VP(S)-SBA15 catalyst) to 25% for the petroleum-extracted V-Porphyrin (i.e., PVP(Oil)-SBA15 sample) after 30 minutes of photoelectrochemical reaction. After 3 h,

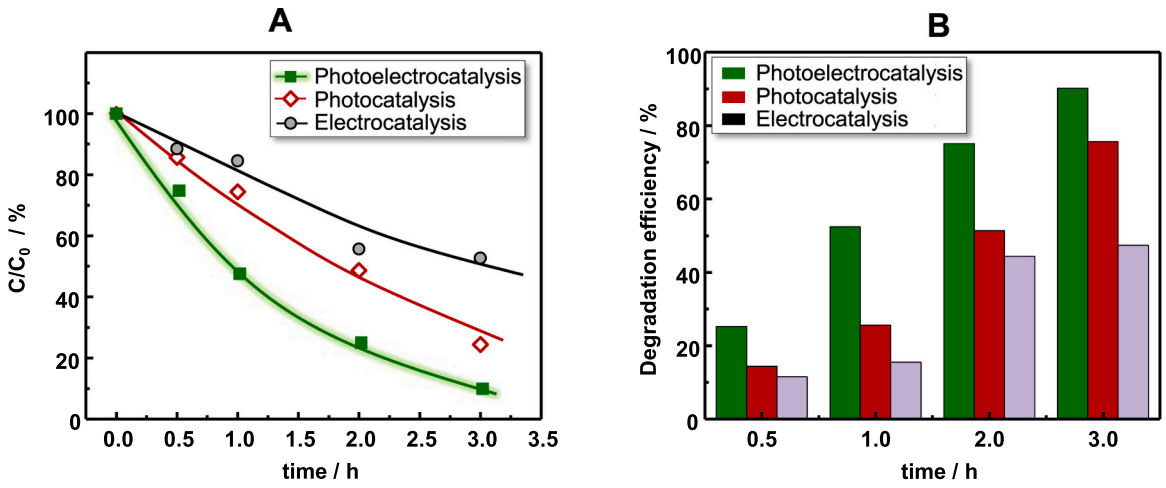

Fig. 9. C/C_0 vs. time plots for methyl red (A) and degradation efficiency (B) for the photoelectro-, photo- and electrocatalytic approaches using a petroleum-extracted vanadyl porphyrin, PVP(Oil)-SBA15.

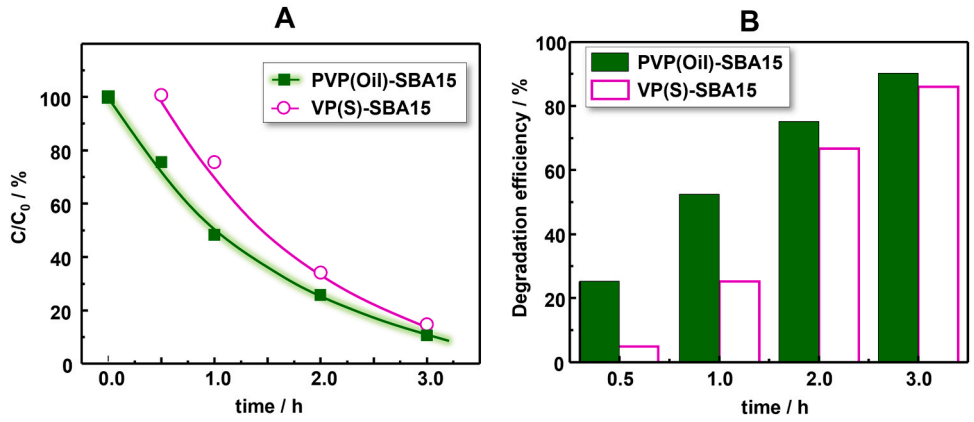

Fig. 10. C/C_0 vs. time plots (A) and degradation efficiency vs. time plots (B) for the photoelectrocatalytic degradation of methyl red using a petroleum-extracted V-porphyrins (PVP(Oil)-SBA15) and a synthetic porphyrin (VP(S)-SBA15) based catalysts.

the PVP(Oil)-SBA15 catalyst almost completely degrades the dye with respect to the 85% dye elimination of the VP(S)-SBA15 catalyst.

We must inform that the supported V-free residue, (R(Oil)-SBA), presents much lower degradation efficiency respect to the corresponding supported primary VP concentrate (PVP(Oil)-SBA), confirming the main role of the vanadyl species in V-porphyrin for this degradation reaction (Fig. S9).

It is important to point out that when considering the variation of the ln (C/C_0) with the reaction time for both VP(S)-SBA15 and VP(Oil)-SBA15 catalysts, and assuming that the photoelectrocatalytic degradation of methyl red followed a pseudo first order kinetics, it can be observed that they should correspond to a straight line from whose slope the pseudo first order kinetic coefficient, k', can be determined (Fig. S10). According with these results, it has been presented the kinetic coefficients together with the R^2 values. The values of R^2 were very close to unity, validating the pseudo first order kinetics assumption for the PEC reaction. In addition, it can be concluded that, an increase of more than 25% in k' was obtained by using the petroleum-extracted based catalyst, i.e., k' of 0.7441 h^{-1} and 0.5882 $h^{-1}$for PVP(Oil)-SBA15 and VP (S)-SBA15 catalysts, respectively.

4. Conclusions

In this study, vanadyl petroporphyrins (VP), extracted from oil (**PVP (Oil)** material) and synthetic (**VP(S)** material), supported on SiO_2 and SBA-15 have been evaluated as potential photoelectrocatalysts. The physico-chemical characterization by FTIR and DR-UV–vis, of the oil derived extract confirms the incorporation of the corresponding vanadyl porphyrins. Furthermore, a comprehensive electrochemical and photoelectrochemical characterization was conducted by EIS, MS and voltammetry tests. From the EIS data, an equivalent circuit was used to obtain the charge transfer resistance at the porphyrin/electrolyte interface, showing the lowest result for the PVP(Oil)-SiO_2 catalyst, which also presented high anodic current density values in the cyclic voltammetries. Besides, PVP(Oil)-containing catalysts presented the highest net current densities in the linear voltammetries under light/dark conditions. In particular, for the PVP(Oil)-SBA15 that was the catalyst presenting the lowest number of defects (MS plots), which is an indicator that defects might act as recombination centres of photogenerated electron and hole pairs. **PVP(Oil)-SBA15** sample was used as a photoelectrocatalyst for the degradation of methyl red showing for the oil extracted (PVP(Oil)-SBA15 catalyst), after 30 min, a degradation efficiency 25% higher than that obtained by the analogous sample based on the synthetic porphyrin (VP(S)-SBA15). Moreover, after 3 h, the PVP (Oil)-SBA15 catalyst could almost completely remove the MR dye, with respect to the 85% of degradation efficiency of the VP(S)-SBA15. According to this, the kinetic constant for PEC-MR-degradation increased more than 25% for the **PVP(Oil)**-containing catalyst compared to the **VP (S)**-containing material, both supported in SBA15.

Declaration of Competing Interest

The authors declare that they have no known competing financial interests or personal relationships that could have appeared to influence the work reported in this paper.

Data availability

Data will be made available on request.

Acknowledgments

The funding received for this study from the Spanish Ministry of Science and Innovation, Projects PID2021–126235OB-C31 and PID2021–126235OB-C33 funded by MCIN/AEI/10.13039/501100011033 and FEDER funds, and from the Ministry of Science and Higher Education of the Republic of Kazakhstan (Project: AP23486934) is acknowledged. This Special Issue is dedicated to honor the 10th International Symposium on Group V (IV and VI) Elements, a gathering of international researchers, industry, young researchers, and students to help shape the vision of the future for these elements.

Appendix A. Supporting information

Supplementary data associated with this article can be found in the online version at doi:10.1016/j.cattod.2024.114855.

References

[1] J.M. Park, J.H. Lee, W.-D. Jang, Applications of porphyrins in emerging energy conversion technologies, Coord. Chem. Rev. 407 (2020) 213157.
[2] M. Strianese, D. Pappalardo, M. Mazzeo, M. Lamberti, C. Pellecchia, The contribution of metalloporphyrin complexes in molecular sensing and in sustainable polymerization processes: a new and unique perspective, Dalton 50 (2021) 7898–7916.
[3] M. Faustova, E. Nikolskaya, M. Sokol, M. Fomicheva, R. Petrov, N. Yabbarov, Metalloporphyrins in Medicine: From History to Recent Trends, ACS Appl. Bio Mater. 3 (2020) 8146–8171.
[4] Sh Shakouri, E. Abouzari-Lotf, J. Chen, Th Diemant, S. Klyatskaya, F.D. Pammer, A. Mizuno, M. Fichtner, M. Ruben, Molecular engineering of metalloporphyrins for high-performance energy storage: central metal matters, ChemSusChem 16 (2023) e202202090.
[5] G. Singh, S. Chandra, Unravelling the structural-property relations of porphyrinoids with respect to photo- and electro-chemical activities, Electrochem. Sci. Adv. 3 (2023) e2100149.
[6] M.M. Pereira, L.D. Dias, M.J.F. Calvete, Metalloporphyrins: Bioinspired Oxidation Catalysts, ACS Catal. 8 (2018) 10784–10808.
[7] X. Li, H. Lei, L. Xie, N. Wang, W. Zhang, R. Cao, Metalloporphyrins as Catalytic Models for Studying Hydrogen and Oxygen Evolution and Oxygen Reduction Reactions, Acc. Chem. Res. 55 (2022) 878–892.
[8] P. Gotico, Z. Halime, A. Aukauloo, Recent advances in metalloporphyrin-based catalyst design towards carbon dioxide reduction: From bio-inspired second coordination sphere modifications to hierarchical architectures, Dalton Trans. 49 (2020) 2381–2396.
[9] W. Zhang, J.J. Dynes, Y. Hu, P. Jiang, S. Ma, Porous metal-metalloporphyrin gel as catalytic binding pocket for highly efficient synergistic catalysis, Nat. Commun. 10 (2019) 1913.
[10] A.M. Ghadiri, M. Farhang, P. Hassani, A. Salek, A.T. Ramezani, A.R. Akbarzadeh, Recent advancements review Suzuki and Heck reactions catalyzed by metalloporphyrins, Inorg. Chem. Commun. 149 (2023) 110359.
[11] R.M. da Silva Jr., E.H. dos Santos, Shi Nakagaki, Metalloporphyrin-based multifunctional catalysts for one-pot assisted Tandem reaction, Mol. Catal. 541 (2023) 113080.
[12] Bh Priya, A.D. Kanika, A.P. Singh, Metalloporphyrins as a catalyst in C–C bond formation, Mater. Today.: Proc. 8 (1) (2023) 853–858.
[13] Y. Kuramochi, A. Satake, Metalloporphyrins: their multitalented nature as observed in multi-metal complex systems, Dalton Trans. 52 (2023) 5418–5422.
[14] G. Piccirillo, M. Moreira-Santos, M. Válega, M.E.S. Eusébio, A.M.S. Silva, R. Ribeiro, H. Freitas, M.M. Pereira, M.J.F. Calvete, Supported metalloporphyrins as reusable catalysts for the degradation of antibiotics: Synthesis, characterization, activity and ecotoxicity studies, Appl. Catal. B-Environ. 282 (2021) 119556.
[15] X.-T. Zhou, H.-B. Ji, X.-J. Huang, Photocatalytic Degradation of Methyl Orange over Metalloporphyrins Supported on TiO_2 Degussa P25, Molecules 17 (2012) 1149–1158.
[16] P. Zhang, J. Hu, B. Liu, J. Yang, H. Hou, Recent advances in metalloporphyrins for environmental and energy applications, Chemosphere 219 (2019) 617–635.
[17] Lucas B. Bolzon, Heide R. Airoldi, Fabrício B. Zanardi, Juliana G. Granado, Yassuko Iamamoto, Metalloporphyrin-functionalized hexagonal mesoporous silica: Synthesis, structural properties and catalytic activity as cytochrome P450 model, Micro Mesop. Mat. 168 (2013) 37–45.
[18] L. Feng, K.-Y. Wang, E. Joseph, H.-C. Zhou, Catalytic Porphyrin Framework Compounds, Trends Chem. 2 (2020) 555–568.
[19] S.S. Rajasree, X. Li, P. Deria, Physical properties of porphyrin-based crystalline metal-organic frameworks, Commun. Chem. 4 (2021) 47.
[20] J. Zhu, X. Chen, A.Q. Thang, F.L. Li, D. Chen, H. Geng, X. Rui, Q. Yan, Vanadium-based metal-organic frameworks and their derivatives for electrochemical energy conversion and storage, SmartMat 3 (3) (2022) 384–416.
[21] L. Feng, K.-Y. Wang, E. Joseph, H.-C. Zhou, Catalytic Porphyrin Framework Compounds, Trends Chem. 2 (2020) 555–568.
[22] J. Zhu, X. Chen, A.Q. Thang, F.L. Li, D. Chen, H. Geng, X. Rui, Q. Yan, Vanadium-based metal-organic frameworks and their derivatives for electrochemical energy conversion and storage. SmartMat 3 (3) (2022) 384–416.
[23] M. Moghadam, I. Mohammadpoor-Baltork, S. Tangestaninejad, V. Mirkhani, A. R. Khosropour, S.A. Taghavi, Electron-deficient vanadium (IV) tetraphenylporphyrin: A new, highly efficient and reusable catalyst for chemoselective trimethylsilylation of alcohols and phenols with hexamethyldisilazane, Appl. Organomet. Chem. 25 (2011) 687–694.
[24] T.A. Dar, B. Uprety, M. Sankar, M.R. Maurya, Robust and electron deficient oxidovanadium (IV) porphyrin catalysts for selective epoxidation and oxidative bromination reactions in aqueous media, Green. Chem. 21 (2019) 1757–1768.
[25] R. Kumar, N. Chaudhary, M. Sankar, M.R. Maurya, Electron deficient nonplanar β-octachlorovanadylporphyrin as a highly efficient and selective epoxidation catalyst for olefins, Dalton Trans. 44 (2015) 17720–17729.
[26] S. Farahmand, M. Ghiaci, Highly selective allylic oxidation of cyclohexene to 2-cyclohexen-1-one under mild conditions over vanadyl-porphyrin implanted onto the aminofunctionalized SBA-15, Microporous Mesoporous Mater. 288 (2019) 109560.
[27] S. Farahmand, M. Ghiaci, S. Asghari, Oxo-vanadium (IV) phthalocyanine implanted onto the modified SBA-15 as a catalyst for direct hydroxylation of benzene to phenol in acetonitrile-water medium: A kinetic study, Chem. Eng. Sci. 232 (2021) 116331.
[28] Zh. K Myltykbayeva, A. Seysembekova, B.M. Moreno, R. Sánchez-Tovar, R. M. Fernández-Domene, A. Vidal-Moya, B. Solsona, J.M. López Nieto, V-Porphyrins Encapsulated or Supported on Siliceous Materials: Synthesis, Characterization, and Photoelectrochemical Properties, Materials 15 (2022) 7473.
[29] D. Tazeev, L. Musin, N. Mironov, D. Milordov, E. Tazeeva, S. Yakubova, M. Yakubov, Complexes of Transition Metals with Petroleum Porphyrin Ligands: Preparation and Evaluation of Catalytic Ability, Catalysts 11 (2021) 1506.
[30] M.L. Chacón-Patiño, J. Nelson, E. Rogel, K. Hench, L. Poirier, F. Lopez-Linares, C. Ovalles, Vanadium and nickel distributions in Pentane, in-between C5-C7 Asphaltenes, and heptane asphaltenes of heavy crude oils, Fuel 292 (2021) 120259.
[31] D. Valencia, Chemical bonding and aromaticity analyzes of petroporphyrins with vanadium or nickel, Fuel 333 (2023) 126344.
[32] G.P. Dechaine, M.R. Gray, Chemistry and Association of Vanadium Compounds in Heavy Oil and Bitumen, and Implications for Their Selective Removal, Energ. Fuel. 24 (2010) 2795–2808.
[33] H. Liu, J. Mu, Z. Wang, Sh Ji, Q. Shi, A. Guo, K. Chen, J. Lu, Characterization of Vanadyl and Nickel Porphyrins Enriched from Heavy Residues by Positive-Ion Electrospray Ionization FT-ICR Mass Spectrometry, Energ. Fuel. 29 (2015) 4803–4813.
[34] P. Ch. Mandal, M. Goto, M. Sasaki, Removal of Nickel and vanadium from Heavy Oils using supercritical water, J. Jpn. Petrol. Inst. 57 (2014) 18–28.
[35] Z. Taherian, A.H.S. Dehaghani, Sh Ayatollahi, R. Kharrat, A new insight to the assessment of asphaltene characterization by using fortier transformed infrared spectroscopy, J. Petrol. Sci. Eng. 205 (2021) 108824.
[36] Y. Zhang, F. Schulz, B. Mc. Rytting, C.C. Walters, K. Kaiser, J.N. Metz, M.R. Harper, Sh.S. Merchant, A.S. Mennito, K. Qian, J.D. Kushnerick, P.K. Kilpatrick, L. Gross, Elucidating the geometric substitution of petroporphyrins by spectroscopic analysis and atomic force microscopy molecular imaging, Energ. Fuels 33 (2019) 6088–6097.
[37] Zh.K. Myltykbaeva, A.V. Anisimov, A.B. Seisembekova, M.B. Smaiyla, Extraction of Vanadylporphyrin Complexes from Oil of the North Buzachi Oil-and-Gas-Bearing Region, Theor. Found. Chem. Eng. 56 (2022) 928–933.
[38] N. Mironov, D. Milordov, E. Tazeeva, D. Tazeev, Guzalia Abilova, Svetlana Yakubova, M. Yakubov, Impact of Asphaltenes on the Adsorption Behavior of Petroleum, Vanadyl Porphyrins: Kinetic and Thermodynamic Aspects, Energy Fuels 35 (2021) 14527–14541.
[39] N.A. Mironov, G.R. Abilova, K.O. Sinyashin, P.I. Gryaznov, Y.Y. Borisova, D. V. Milordov, E.G. Tazeeva, S.G. Yakubova, D.N. Borisov, M.R. Yakubov, Chromatographic Isolation of Petroleum Vanadyl Porphyrins Using Sulfocationites as Sorbents, Energy Fuels 32 (2018) 161–168.
[40] M.R. Maurya, V. Prakash, Il Yadav, M. Sankar, Effect of para-Substituents on meso-Functionalized Oxidovanadium(IV) Porphyrins as Catalysts for Oxygen Atom Transfer Mediated Oxidation of Benzoin to Benzil under Mild Conditions, Eur. J. Inorg. Chem. 26 (2023) e202300374.
[41] M.R. Maurya, V. Prakash, F. Avecilla, M. Sankar, Selective Bromination of β-Positions of Porphyrin by Self-Catalytic Behaviour of VOTPP: Facile Synthesis, Electrochemical Redox Properties and Catalytic Application, Eur. J. Inorg. Chem. 17 (2021) 1685–1694.
[42] J.L. Appleton, N. Le Breton, M.-A. Carvalho, J. Weiss, A.K. Boudalis, Ch Gourlaouen, S. Choua, R. Ruppert, Vanadyl(IV) Porphyrin Dimers with

Palladium(II) and Platinum(II) Linkages: Syntheses, Electronic Properties, and Magnetic Interactions between the Two Moieties, Cryst. Growth Des. 23 (2023) 1689–1696.
[43] Y. Ruan, B. Gao, Synthesis of zinc-porphyrin based multi-arm star Poly (Nisopropylacrylamide) and the effect of topology on photocatalytic performance, J. Mol. Struct. 1210 (2020) 128050.
[44] Y. Wang, L. Zhao, G. Ji, Ch He, S. Liu, Ch Duan, Vanadium(VIV)–Porphyrin-Based Metal–Organic Frameworks for Synergistic Bimetallic Activation of Inert C(sp3)–H Bonds, ACS Appl. Mater. Interfaces 14 (2022) 2794–2804.
[45] S.M.L. Santos, J.A. Cecilia, E. Vilarrasa-García, I.J. Silva Junior, E. Rodríguez-Castellón, D.C.S. Azevedo, The effect of structure modifying agents in the SBA-15 for its application in the biomolecules adsorption, Microporous Mesoporous Mater. 232 (2016) 53–64.
[46] Y.Y. Borisova, E.G. Tazeeva, N.A. Mironov, D.N. Borisov, S.G. Yakubova, G. R. Abilova, K.O. Sinyashin, M.R. Yakubov, Role of Vanadylporphyrins in the Flocculation and Sedimentation of Asphaltenes of Heavy Oils with High Vanadium Content, Energ. Fuels 31 (2017) 13382–13391.
[47] J.R. Kincaid, M.W. Urban, T. Watanabe, K. Nakamoto, Infrared spectra of matrix-isolated metal complexes of octaethylporphine, J. Phys. Chem. 87 (1983) 3096–3101.
[48] X. Zhao, Y. Liu, C. Xu, Y. Yan, Y. Zhang, Q. Zhang, S. Zhao, K. Chung, M.R. Gray, Q. Shi, Separation and Characterization of Vanadyl Porphyrins in Venezuela Orinoco Heavy Crude Oil, Energ. Fuels 27 (2013) 2874–2882.
[49] M. Yakubov, G. Abilova, E. Tazeeva, S. Yakubova, D. Tazeev, N. Mironov, D. Milordov, A Comparative Analysis of Vanadyl Porphyrins Isolated from Resins of Heavy Oils with High and Low Vanadium Content, Processes 9 (2021) 2235.
[50] X. Wang, Sh Li, L. Zhao, Ch Xu, J. Gao, A DFT and TD-DFT study on electronic structures and UV-spectra properties of octaethyl-porphyrin with different central metals (Ni, V, Cu, Co), Chin. J. Chem. Eng. 28 (2020) 532–540.
[51] N.A. Mironov, G.R. Abilova, Y.Y. Borisova, E.G. Tazeeva, D.V. Milordov, S. G. Yakubova, M.R. Yakubov, Comparative Study of Resins and Asphaltenes of Heavy Oils as Sources for Obtaining Pure Vanadyl Porphyrins by the Sulfocationite-Based Chromatographic Method, Energy Fuels 32 (2018) 12435–12446.
[52] H. Xu, G. Que, Da Yu, J.R. Lu, Characterization of Petroporphyrins Using Ultraviolet-Visible Spectroscopy and Laser Desorption Ionization Time-of-Flight Mass Spectrometry, Energ. Fuels 19 (2005) 517–524.
[53] P. Ch. Mandal, N. Wahyudiono, M. Sasaki, M. Goto, Non-catalytic vanadium removal from vanadyl etioporphyrin (VO-EP) using a mixed solvent of supercritical water and toluene: A kinetic study, Fuel 92 (2012) 288–294.
[54] V. Ramachandran, J. van Tol, A.M. McKenna, R.P. Rodgers, A.G. Marshall, N. S. Dalal, High Field Electron Paramagnetic Resonance Characterization of Electronic and Structural Environments for Paramagnetic Metal Ions and Organic Free Radicals in Deepwater Horizon Oil Spill Tar Balls, Anal. Chem. 87 (2015) 2306–2313.
[55] D. Gourier, O. Delpoux, A. Bonduelle, L. Binet, I. Ciofini, H. Vezin, EPR, ENDOR, and HYSCORE Study of the Structure and the Stability of Vanadyl-Porphyrin Complexes Encapsulated in Silica: Potential Paramagnetic Biomarkers for the Origin of Life, J. Phys. Chem. B 114 (2010) 3714–3725.
[56] D. Mannikko, S. Stoll, Vanadyl Porphyrin Speciation Based on Submegahertz Ligand Proton Hyperfine Couplings, Energy Fuels 33 (2019) 4237–4243.
[57] F.-Q. Xiong, L. Wan, Y. Li, T. Thomas, F.J. DiSalvo, M. Yang, Crucial Role of Donor Density in the Performance of Oxynitride Perovskite $LaTiO_2N$ for Photocatalytic Water Oxidation, ChemSusChem 10 (2017) 930–937.
[58] G. Sánchez-García, E. Da Silva, R.M. Fernández-Domene, A. Cháfer, V. González-Alfaro, B. Solsona, R. Sánchez-Tovar, TiO_2 nanostructures synthesized by electrochemical anodization in green protic ionic liquids for photoelectrochemical applications, Ceram. Int 49 (2023) 26900–26909.
[59] A. Galenda, L. Crociani, N.El Habra, M. Favaro, M.M. Natile, G. Rossetto, Effect of reaction conditions on methyl red degradation mediated by boron and nitrogen doped TiO_2, Appl. Surf. Sci. 314 (2014) 919–930.
[60] J.E.L. Santos, D.R. da Silva, C.A. Martínez-Huitle, E.V. Dos Santos, M.A. Quiroz, Cathodic hydrogen production by simultaneous oxidation of methyl red and 2,4-dichlorophenoxyacetate aqueous solutions using Pb/PbO_2, Ti/Sb-doped SnO_2 and Si/BDD anodes. Part 1: electrochemical oxidation, RSC Adv. 10 (2020) 37695–37706.